The Nature and Impacts of Fines in Smelter Grade Alumina

AUTHORS

Linus Perander[1], Zoran Zujovic[2], Tom Kemp[3], Mark Smith[3], James Metson[1,2]

[1)] Light Metals Research Centre, University of Auckland, Private Bag 92019, Auckland, New Zealand
[2)] Department of Chemistry, University of Auckland, Private Bag 90219, Auckland, New Zealand
[3)] Department of Physics, University of Warwick, Coventry CV4 7AL, United Kingdom

ABSTRACT

Fines in smelter grade aluminas are recognised as a significant process problem in aluminium smelting. However the understanding of the nature of this fine material and how it impacts on the reduction process are less clearly understood. The combination of new analytical methods such as Variable Pressure Scanning Electron Microscopy and very high field Solid State NMR provide new insights into the spatial distribution of phases within aluminas, and suggest how such fine materials are generated, particularly during calcination in the alumina refinery.

INTRODUCTION

The bulk of the alumina produced for the smelting of aluminium is produced by the Bayer process [1]. Gibbsite $Al(OH)_3$ grows by precipitation and agglomeration in the clarified Bayer liquor and is subsequently recovered by filtration and calcined to form smelter or "metallurgical grade alumina (SGA). The isomorphous transformation from Gibbsite to alumina leaves a similarly aggregated, polycrystalline material. The break-up of this aggregated material in any of the handling processes in filtration, calcination and transport leads to the inevitable formation of finer material than the initial particle size distribution recovered from precipitation. Importantly, this attrition continues through the handling of the alumina at the smelter before it reaches the reduction cell. Taylor et al. provide profiles of this attrition for a number of smelters [2]. When it comes to understanding or predicting the behaviour of an alumina in the reduction process, the nature of the fine (<40μm) and ultra-fine (<20μm) size fractions can be particularly revealing.

Although the chemical purity of SGA is often very high (often more than 99.7% Al_2O_3) the microstructure is typically highly disordered, with large variations between, and even within, individual particles, as discussed below. The tolerances for alumina purity are fairly strict however the variation in microstructure less regulated, partly because it is not easy to measure and report, and is considered less relevant in the smelter. Nevertheless, there is considerable evidence that particularly in the case of fine materials, not only their presence, but their composition and microstructure, have significant impacts on the reduction process.

In this paper we explore the nature and origin of these variations in the distribution of alumina phases between different sized particles.

IMPACTS OF CALCINATION ON FINES

The analysis of the bulk SGA sample provides only a limited picture of the material. For example, impurity phases and even a high alpha alumina content in the fine particles are averaged out and barely noticed in x-ray diffraction (XRD) based analysis of the bulk material. Yet there is every reason to expect differences in phases with particle size. For some calcination technologies, finer particles are retained longer in the hot zone in the furnace, due to internal recirculation, or the flow characteristics of the fine versus the coarse particles. Even if the phase transformation reactions from transition alumina to the thermodynamically stable alpha alumina are slow, the longer heating times will inevitably result in a higher content of alpha alumina in the smaller size fractions. For similar retention times, the increased area for heat transfer in small particles may also effect the phase transformation reaction and hence the conversion to alpha alumina. This effect becomes very obvious when a 'typical' alumina is size fractionated and the various fractions studied by XRD (**figure 1**). When moving to finer size fractions the alpha alumina content, indicated by the sharp reflections in the diffractograms, increases significantly. It is also interesting to note, in this example, the additional peak (at around 15-16° 2theta) observed only for the intermediate size fractions, which indicates the presence of an additional impurity phase.

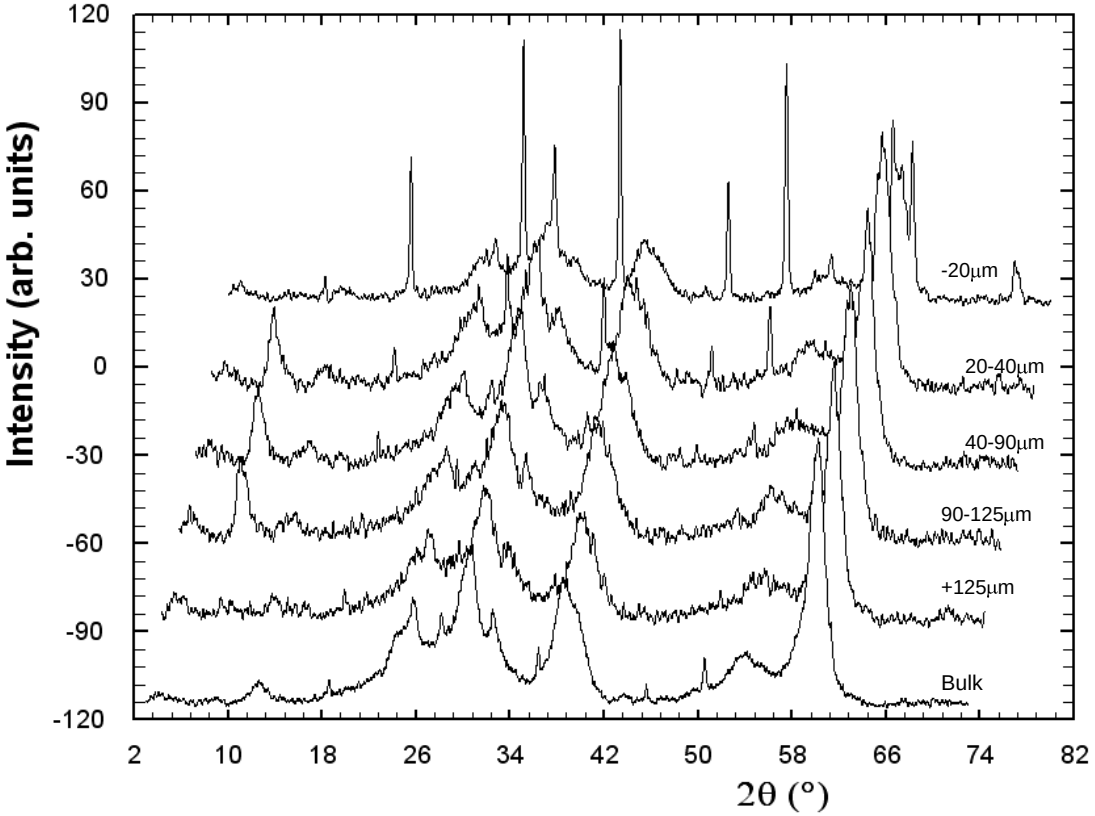

Figure 1. X-ray diffractograms for a size fractionated smelter alumina. From front to back: bulk, plus 125 μm, 90-125μm, 40-90μm, 20-40μm and minus 20μm. Note that the alpha alumina (indicated by the sharp and narrow peaks) content is increasing in the finer size fractions.

The particle size distribution of the gibbsite going in to the calciner and the final product coming out is not the same. Despite the best efforts in design and operation, some of the fines are generated in the calciner which may increase the alpha alumina content of the alumina. This particle breakage is both influenced by the calciner technology and the strength of agglomeration of the original gibbsite [3]. Agglomerates break up into smaller fragments due to mechanical forces or thermal shock when contacting hot gases or solids. Furthermore, during the phase transformation of the Gibbsite into alumina, the crystallites shrink (largely along the c-axis direction in the gibbsite lattice) which can cause further mechanical stress in the particles and fragmentation. The alumina particles will also break up due to mechanical forces from collisions between the particles themselves or between particles and other surfaces.

The cross sectioned alumina particle to the left in **figure 2** provides an example of the effect of the c-axis shrinkage in an agglomerated particle. In the gibbsite particles the crystallites may have different orientations (reflected in the morphology which can be radial or mosaic/agglomerated) depending on the mechanism of particle growth and how the precipitation stage is operated. When gibbsite reacts to form the transition aluminas and the crystallites shrink, cracking can occur at the crystallite/grain boundaries. Also of note in the figure is the charge contrast that occurs at the perimeter of the particle. In the ESEM the denser, structurally more ordered, alpha alumina phase results in a difference in the observed charge contrast as compared to the intermediate and more amorphous transition aluminas. This shows up as the bright white features in the images. The charge contrast phenomenon, unique to the Environmental and Variable Pressure SEM, occurs due to differences in the materials ability to dissipate the charge build-up experienced by uncoated samples under the electron beam. Charge contrast imaging, and its implications for studying smelter grade alumina, is discussed in more detail elsewhere [4].

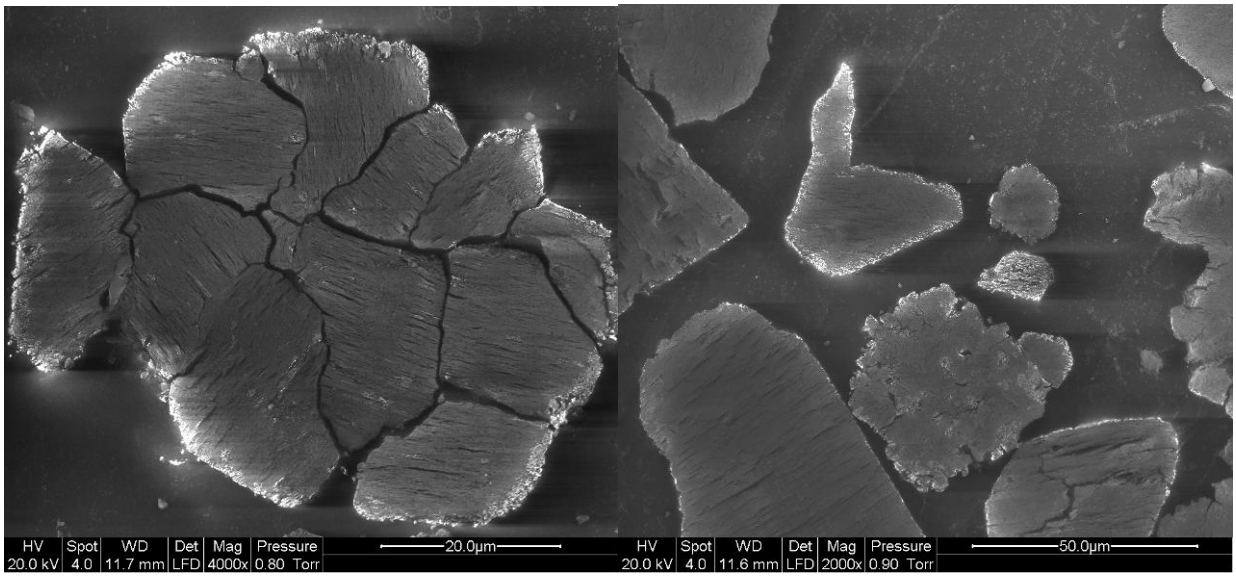

Figure 2. A cross-sectional Scanning Electron Microscope image of a smelter alumina particle. Shrinkage in the gibbsite c-axis direction leads to cracking between the crystallites. Note also the alpha alumina at the perimeter and along some of the internal boundaries of the particle.

Not surprisingly, there appears to be a difference in the distribution of the alpha alumina phase for material produced by different calcination technologies. For the modern gas suspension, fluid flash or circulating fluid bed calciners the alpha alumina seems to be preferentially located at the outer surface of the particles, compared to the rotary kiln calcined aluminas where a more even distribution is observed. This indicates that the high heating rates and short residence times in the modern calciners lead to structural variations not only between particles, but also within them. Another possible consequence of the shell formation is that the particles may crack due to a build-up of internal vapour pressure as the water generated in the phase transition is released from the structure. It is also interesting to speculate on what an alpha alumina shell means for the alumina properties in the smelter. It is probable that particularly the kinetics of HF-scrubbing and the dissolution properties are influenced by these compositional variations.

In the smelter, the presence of large amounts of alpha alumina in the fine particles can be problematic for a number of reasons:

- Dispersion, dissolution and sludge formation due to the slower dissolution of alpha alumina and the tendency for fine particles to stick together.

- Crust formation and crust evolution as the compositional variations in the alumina is likely to influence the strength of the crust and the reactions in the crust as it picks up HF and bath vapours.

- Alumina flowability and handling, since the flow characteristics for alpha alumina fines (or material with large amounts of fines mixed into it) are very different, transportation and handling becomes more difficult. Segregation effects can also occur, which further amplifies the detrimental effects of the alpha alumina laden fines.

- Feed control may also be compromised (especially for volumetric point fed cells) due to segregation and density differences for material with large amounts of alpha alumina fines.

CCI in the ESEM can be a very useful technique to investigate the distribution of alpha alumina between particles and also within particles as it allows direct observation of alpha alumina distribution in cross sectioned particles. As can be seen from the image above (**figure 2**) it is relatively easy to discern the over-calcined fine alumina particles. Notice also the shape of the larger of the over-calcined particles; clearly a fragment of a larger particle. Particle morphology or shape is another important factor for the flowability of the material.

THE NATURE OF UNDER CALCINED FINES

As the size and energy efficiency of calciners increases, under- (boehmite, chi-alumina, gamma-alumina) or un-calcined (gibbsite) particles might be anticipated to be more prevalent in some technologies. For example, alumina fines from refineries using gas suspension or fluid flash calciners, are expected to differ in phase composition from those in refineries equipped with

circulating fluidised bed or rotary kiln calciners where fines are more highly calcined. In most technologies,the gibbsite dust is expected to come predominantly from the ESP filters and may include material that has by-passed the calcination stage altogether. As the structure is well ordered, gibbsite, even at low levels, is expected to be detected in the X-ray diffractograms of the bulk material and is frequently reported on the specification sheet. In the aluminium smelter, gibbsite containing dust is detrimental as it can cause:

- Increased dusting
- Loss of bath
- A direct decrease in the alumina content available for reduction
- Additional HF formation
- Cell instability

Gibbsite ($Al(OH)_3$) remains relatively stable at temperatures up to 250°C, before it starts to convert to boehmite and/or the transition aluminas (depending on the reaction conditions). This means that, unlike the transition aluminas, the hydroxyls are retained even if the material is pre-heated (in the hoppers or feeders) before being fed into the cell. For the transition aluminas a significant part of the adsorbed water (in the form of loosely bound, or physisorbed, surface species) are removed when the material is heated. This relatively labile exchange is also reflected in the location specific MOI values [5]. The LOI values reflect the loss of the residual structural hydroxide species which are essential to the structures of the transition aluminas. The comparison is seen in the thermograms below (**figure 3**).

The effect of gibbsite in the SGA is that a large amount of hydrogen enters the cell with the material in the form of hydroxyls in the gibbsite. By weight approximately 35% of the gibbsite will react to form H_2O (which also means that there is less alumina available for metal production!). Once the material is heated, this water loss will occur very rapidly when such particles come in contact with the bath, and the hydroxide reacts to form H_2O and Al_2O_3. The near explosive formation of large amounts of water vapour may then carry fine particles back up the feeder hole (volcano effect) increasing dusting.

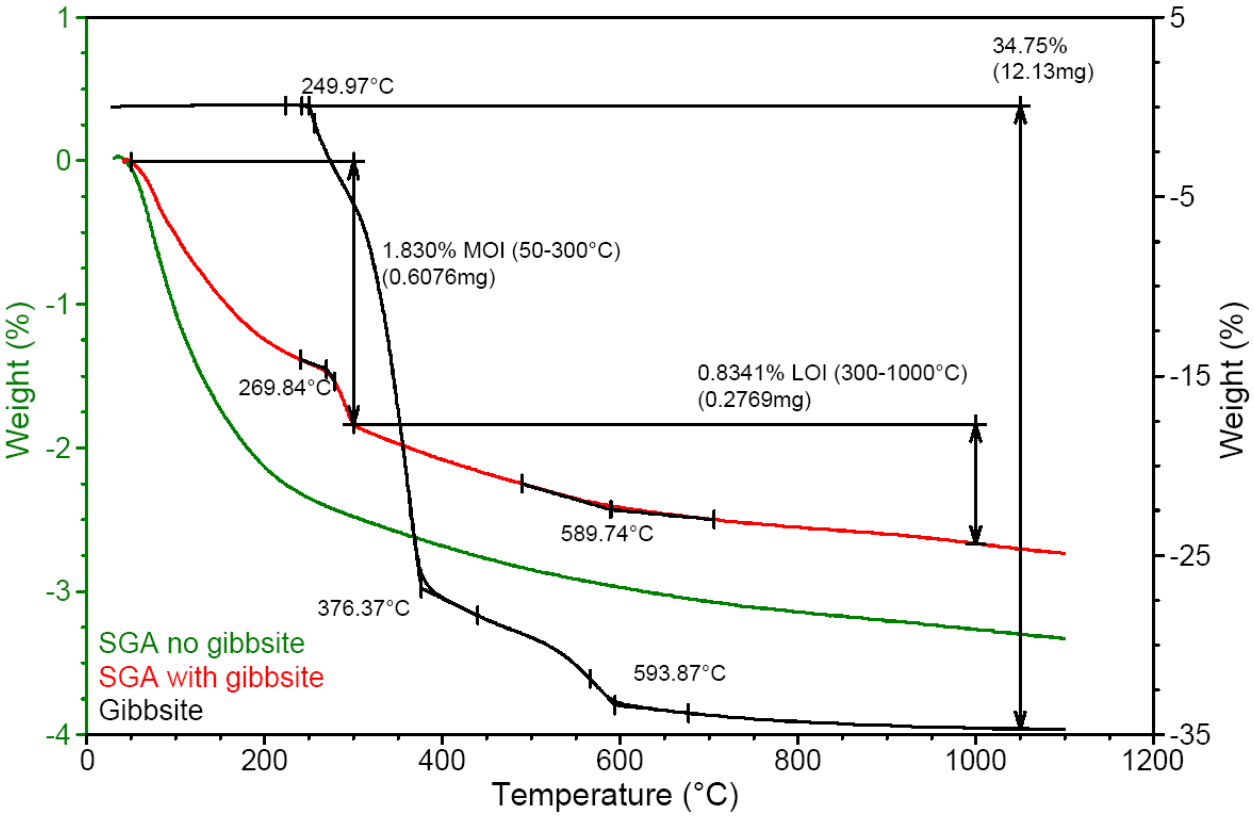

Figure 3. Thermograms of pure Bayer gibbsite (black line, right y-axis) and two smelter grade aluminas: with no gibbsite (green line, left y-axis) and with residual gibbsite (red line, left y-axis).

The presence of gibbsite in the alumina will also have a small impact on the energy consumption and thermal balance of the cell. Compared to the dissolution of alumina, which requires 106-130 kJ per mole of Al_2O_3 [6], the reaction of gibbsite to transition alumina (reaction 1):

$$2Al(OH)_3(s) \rightarrow Al_2O_3(s) + 3H_2O(g) \quad (1)$$

requires about 260 kJ of energy per mole of gibbsite [7]. In both cases, another 90-112 kJ of energy per mole of Al_2O_3 is needed to lift the temperature to the electrolyte temperature at which it dissolves [6].

Another consequence of gibbsite in the fines (or bulk for that matter) is that this also has direct process and economic impacts is the loss of bath through the formation of HF. Water (or hydroxyls or hydrogen) introduced to the bath (in any form) has the potential to react to form HF, according to reactions 2 and 3 [8]:

$$2AlF_3 \text{ (g or diss)} + 3H_2O(g) \rightarrow 6HF(g) + Al_2O_3(s \text{ or diss}) \quad (2)$$
$$3H_2O(g) + 3NaAlF_4(g) \rightarrow 6HF(g) + Al_2O_3(s) + Na_3AlF_6(s) \quad (3)$$

Compared to surface water, much of which is lost before dissolution, the hydroxyl (OH) is a much more potent HF source [9]. Even a few percent of gibbsite would add significantly to the

total HF burden. The capture efficiency of the fluoride containing duct gases/particles is high, however this circuit fails to capture all the volatiles and particulates lost into the potroom, so such fluoride losses become significant and can be problematic also in the quality of the working environment. The lost electrolyte will have to be supplemented by additional AlF_3 which is another direct financial loss. The increased HF generation from the OH in gibbsite introduces a further challenge in meeting increasingly stringent emission limits.

As seen in **figure 3**, thermo gravimetric analysis (TGA) can be used to qualitatively detect even small amounts (<1 wt-%) of gibbsite in the alumina. However, to quantify the gibbsite (and estimate the financial and environmental impacts) XRD analysis with Rietveld refinement is a far more useful technique. Gibbsite is a highly crystalline material and even small amounts in the bulk gives rise to detectable peaks. The distribution of gibbsite in the various size fractions can readily be studied by analysing sieved material. As with alpha alumina, for particular calcination technologies the gibbsite content is higher in the fine size fraction. Depending on how the ESP dust is treated, boehmite (AlOOH) can also be present. In **figures 4 and 5** the X-ray diffractograms and Rietveld refinements of the bulk and the sub 40 micron size fraction for an industrial alumina sample are displayed and the quantitative results can be seen in **table 1**.

Table 1. XRD results.

	GoF*	gibbsite	boehmite	total-gamma**	theta	alpha
	Chi^2	(wt-%)	(wt-%)	(wt-%)	(wt-%)	(wt-%)
Bulk	0.49	1.2	N/A	54.9	24.1	19.8
<40μm	0.16	22.0	4.9	35.7	20.4	17.0

*) GoF, goodness of fit, a measurement of the quality and accuracy of the Rietveld refinement (<1 is generally considered to be a reasonable fit).
**) Refers to the total gamma alumina content, including both the gamma and the gamma-prime phases.

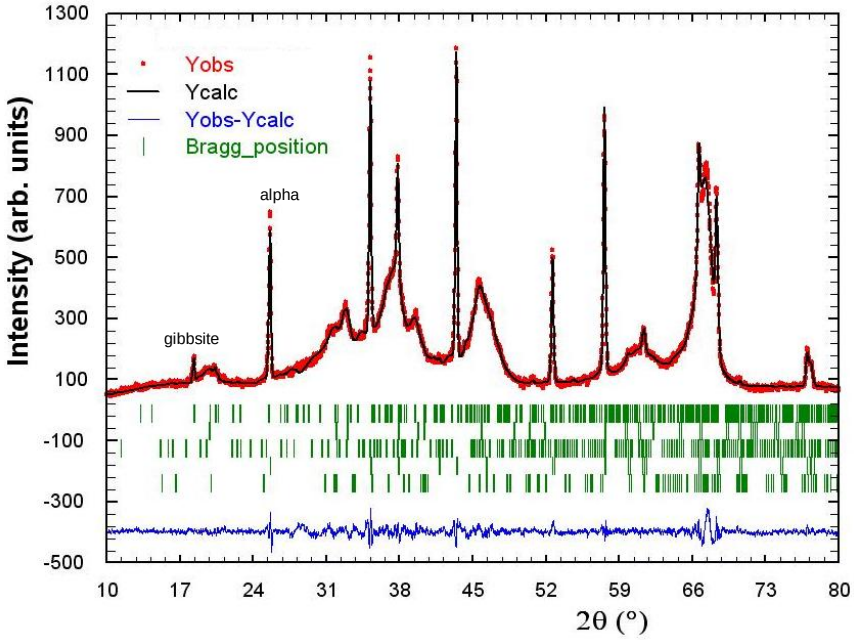

Figure 4. X-ray diffractogram and Rietveld profile refinement for an industrial alumina (bulk). Some characteristic peaks are indicated in the diagram.

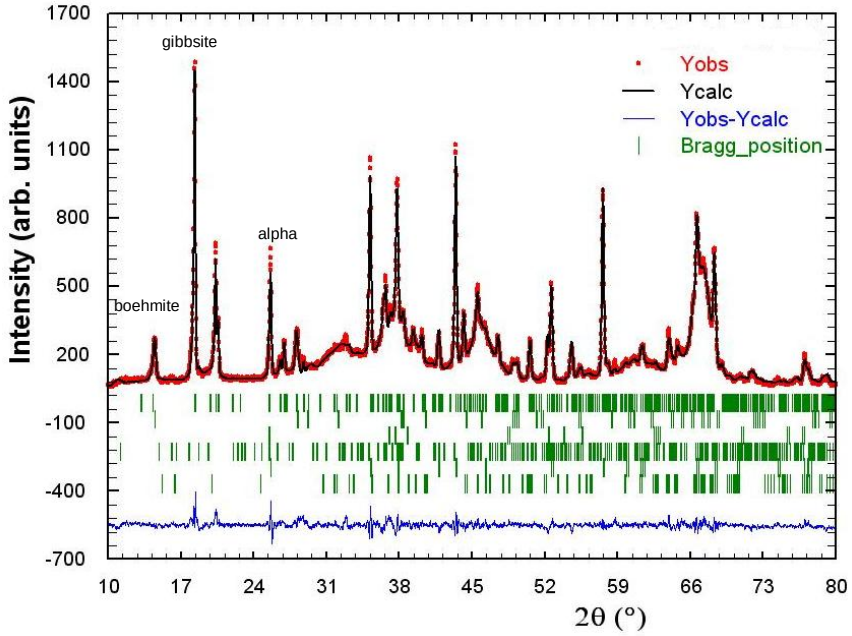

Figure 5. X-ray diffractogram and Rietveld refinement for an industrial alumina (<40μm size fraction). Some characteristic peaks are indicated in the diagram.

Another very useful technique for detecting the presence of under calcined material is the measurement of pore size distribution. The pore size distribution can be evaluated at the same time as the better established BET specific surface area measurements [10], by analysing the adsorption branch of the isotherm using the BJH method [11]. The pore size is very much a function of the degree of calcination. When heated, adjacent hydroxyls in the gibbsite react through a proton capture mechanism to form water that diffuses out via the structural channels in the gibbsite lattice; this also forms the nucleus of a pore. During the early stage of the calcination reaction the pore density is high and average size is less than 2 nm, resulting in the very high specific surface areas (up to 350 m^2g^{-1} and above). The progressive loss of hydroxyl groups, and the structural rearrangement that accompany this, result in an expansion of the pore size. The bimodal distribution seen in **figure 6** indicates an alumina with two distinct pore populations indicating a mixture of microporous (high surface area, small pore size, low degree of calcination) and mesoporous (lower surface area material, larger pore size) materials. When performing BET surface area and BJH pore size distribution measurements on the aluminas, special care has to be taken in the preparation so as not to induce phase transformation during pre-treatment. For example, the typical degas temperature of 200°C, often used in the industry, is high enough to alter phase distribution and thus also the pore size.

The alumina pore size distribution may have implications for dry-scrubber performance as it is critical in providing access to internal surfaces and reactive sites. An interesting question that arises from this is if the small pores are as accessible to HF on the same time scale as the larger pores. Also of note is that the material with the smaller pore size has a larger surface area, thus contributing more to the total surface area (as reported on the specifications sheet).

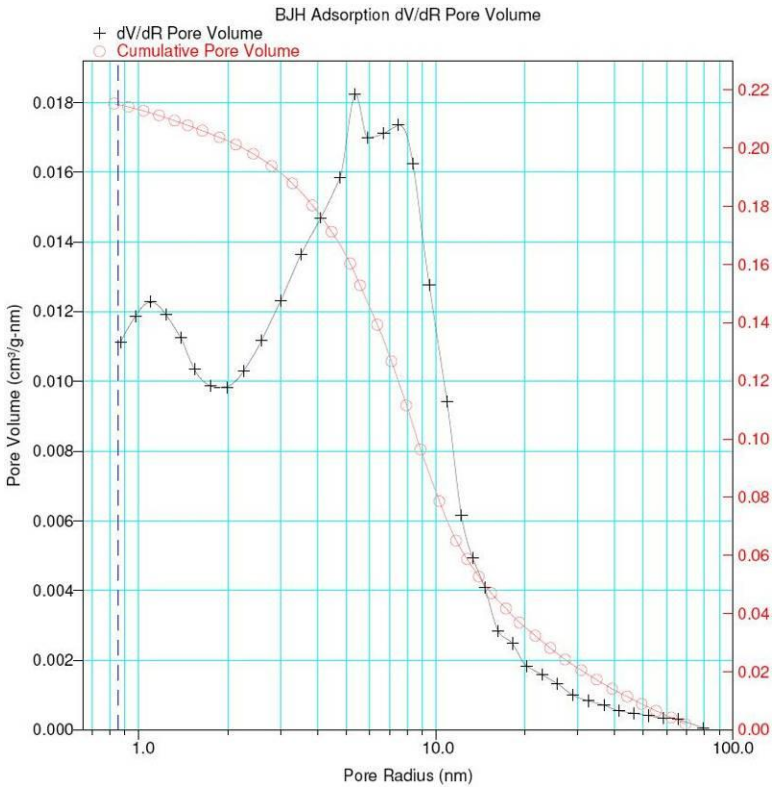

Figure 6. Pore size distribution measurement revealing a mixture of microporous (high surface area, small pore size) and mesoporous (lower surface area material, larger pore size) materials.

A MORE COMPLEX PROBLEM?

The microstructure of smelter aluminas is particularly complex relative to their compositional analysis. The more amorphous transition alumina phases, (not gibbsite or alpha-alumina) comprise the bulk of the material, and have a large influence on the properties and thus performance of the alumina in the smelter – for example the influence on the dissolution characteristics. These phases are however notoriously difficult to characterise, using 'conventional' techniques, such as laboratory based XRD, due to their lack of crystallographic long range order. Structural analysis of SGA is further complicated by the co-existence of a wide range of these transition alumina phases [12].

These 'amorphous' phases are important in the dissolution process and for crust formation and stability. Physi- and chemisorbed surface water or hydroxyl aid the dissolution process by improving the dispersion of alumina on and in the bath. The transition aluminas also contribute the large surface area critically important for HF adsorption and scrubbing capacity. The trade-off however is increased formation of HF from structural hydroxyl species introduced into the electrolyte with aluminas of higher surface area. Indeed the 'residual hydroxyl' has been considered to be the main source of HF formation in the smelter [8].

There is clearly a need to understand not only the amount, but also the distribution of the transition alumina phases in the SGAs in order to fully understand and predict performance

characteristics. ESEM and TEM are particularly useful techniques as they allow the distribution of phases within cross sectioned particles to be studied. As discussed in more detail elsewhere [4], the charge contrast phenomena in the ESEM allows particularly alpha to be 'seen'. For long term soak calcined samples, the alpha alumina generally show a distribution that correlates with the gibbsite *growth rings* (see the papers by Roach et al and Baroni et al [13, 14]) which hints towards a impurity or defect catalysed mechanism for the transformation reactions (**figure 7, left**). This banding is attributed to variations in Na concentration associated with the cycling of gibbsite particles through precipitation as they grow to sizes harvestable in product filtration. As could be seen in **figure 2**, rapid- or flash calcined samples often display a preferential distribution of alpha alumina around the outer surface/perimeter of the particle, possible a result of heat and mass transfer limitations due to the short calcination times and rapid heating rates (**figure 7, right**). Examination of cross sectioned alumina grains also can reveal the presence of inclusions within the particles **(figure 8**).

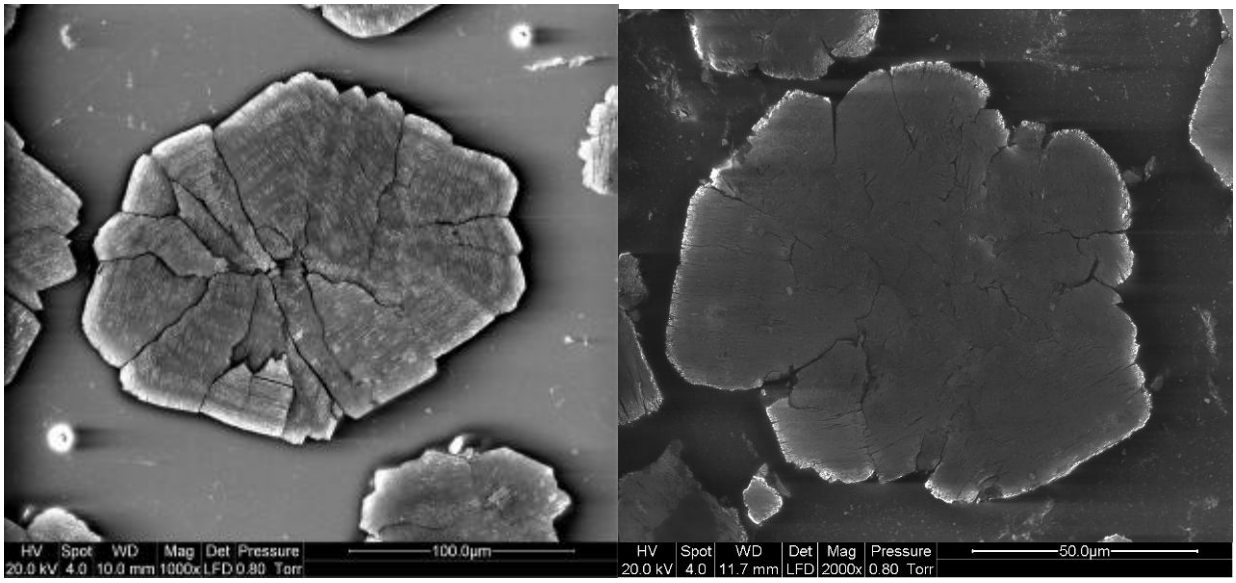

Figure 7. Left Image: Soak calcined cross sectioned alumina grain with high alpha alumina content (similar to what is achieved in some rotary kiln calcination operations), Right Image: cross sectioned Gas Suspension calcined alumina grain.

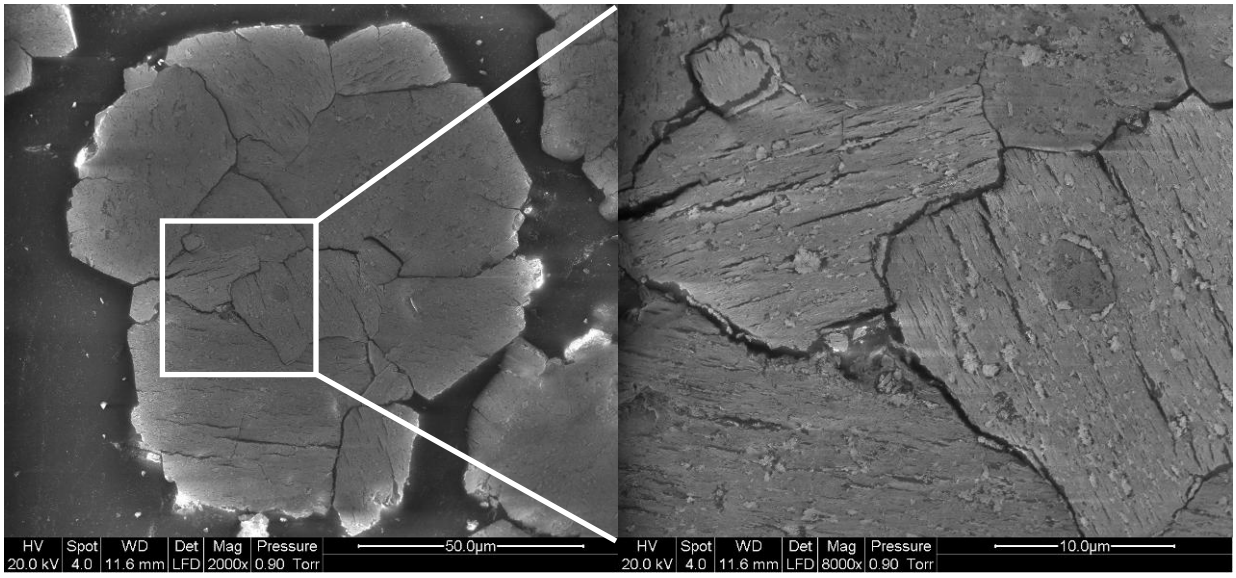

Figure 8. Left Image: Cross sectioned alumina grain displaying the presences of small inclusion possible filter back wash or scales incorporated in the alumina matrix, Right Image: Enlargement of a selected area.

Another technique that shows considerable promise for examining SGAs is Solid State Magic Angle Spinning NMR (SS MAS NMR) [15]. SS MAS NMR studies gives insight into the structural co-ordination of all the aluminium ions in the structure, irrespective of long range ordering [16], which is key to understanding the forms of alumina. Chemical shift ranges for aluminium in different coordinations with oxygen (or hydroxyls) are typically −10 to 20 ppm for octahedrally coordinated aluminium (AlO_6), 30 to 40 ppm for pentahedrally coordinated aluminium (AlO_5) and 50 to 80 ppm for tetrahedrally coordinated aluminium (AlO_4) [16, 17]. Several NMR studies explore the transition aluminas [17-21] but the technique has not yet been widely applied to SGAs. The co-existence of the different transition alumina phases and the influence of the second-order quadrupolar interaction cause spectral broadening; however the availability of higher magnetic fields allows some of these problems to be overcome [22].

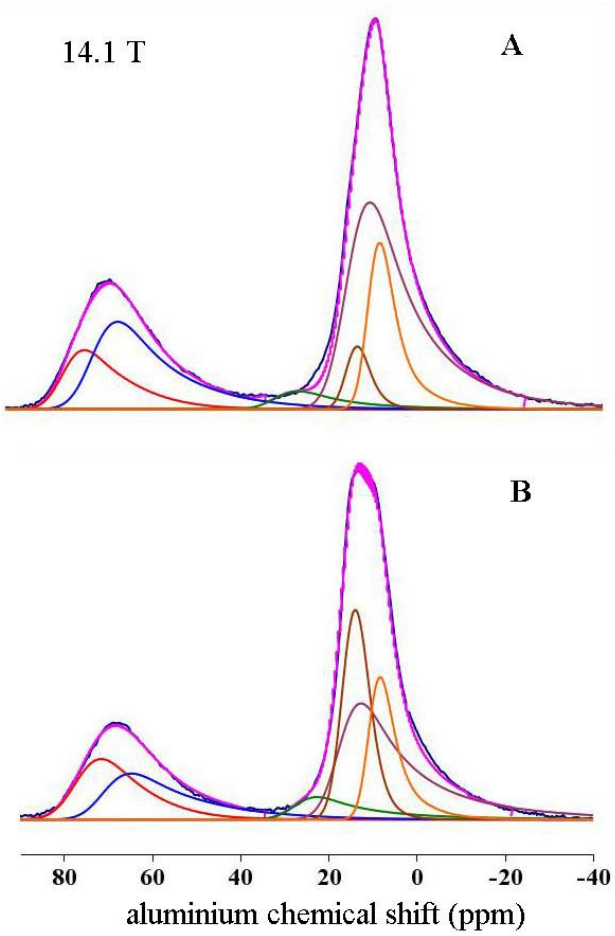

Figure 9. SS-NMR results from an industrial alumina sample A) bulk material, B) <40μm fraction. The blue line is the experimental spectrum and the magenta line is the sum of the individual fitted curves. Note that the experiments were run and fitted at three different magnetic field strengths (important for the robustness of the method) although only the 14.1 T results are shown here.

The ^{27}Al SS MAS NMR spectra at 14.1 T obtained on both the bulk (A) and sub 40 μm size fraction (B) of an industrial alumina sample are shown in **figure 9**. The NMR parameters and relative abundance (intensities) of each site are shown in **table 2**. The key to the robustness and uniqueness of these fits, despite the significant spectral overlap, is that the experiments and fits are performed at different magnetic field strengths (7.1 T, 11.7 T and 14.1 T) and that the same parameters are used to fit the spectra at all fields. The ability to fit all three fields accurately with spurious parameters would be highly coincidental and is hence unlikely. Also the positions (and parameters) of several of the peaks are not arbitrary as they are largely determined by the known phases that are present in this sample on the basis of the x-ray evidence (i.e. gamma-, theta- and alpha-alumina).

Table 2. Peak parameters used in the curve fitting of the NMR data, collected at 7.1, 11.7 and 14.1 T, for an industrial alumina sample and the resulting peak intensities.

	^{27}Al NMR Peak	Chemical Shift /ppm	Mean C_Q / MHz (± 1 MHz)	ΔC_Q / MHz (± 1 MHz)	Alumina Intensity / %	Alumina Phase

Bulk (A)	Tetrahedral 1	79.5(0.5)	6.5	4.0	12(1)	Theta
	Tetrahedral 2	71.5(0.5)	7.0	6.0	20(0.1)	Gamma
	*Pentahedral	32(1)	6.0	7.0	5(2)	**
	Octahedral 1	15.5	6.0	7.0	43(1)	Gamma
	Octahedral 2	14.5(0.5)	2.5	3.5	4.5(0.5)	Alpha
	Octahedral 3	9.5(1)	3.0	5.5	14.5(1.5)	Theta
< 40 μm (B)	Tetrahedral 1	78(1)	6.5	4.0	13.5(0.5)	Theta
	Tetrahedral 2	72(1)	8.0	6.0	15(1)	Gamma
	*Pentahedral	28(1)	6.0	10.0	7(2)	**
	Octahedral 1	16(1)	6.0	10.0	28(2)	Gamma
	Octahedral 2	15.5(0.5)	2.5	3.5	21(0.5)	Alpha
	Octahedral 3	9.5(0.5)	3.0	5.5	13.5(1.5)	Theta

*) Possibly a quasi-octahedral peak (see discussion)

**) Small quantity of AlO_5 from some less ordered component of gamma- or other transition alumina (such as the more X-ray amorphous chi- or rho-aluminas).

The peaks centred at a chemical shift of approximately 30 ppm, could either indicate the presence of quasi-octahedral [15, 23] or pentahedral (AlO_5) aluminium coordination in accordance with previously reported values for the chemical shift [17, 24, 25]. However, the higher value of C_Q and ΔC_Q more likely indicates the presence of pentahedral coordination. C_Q is the quadrupole coupling constant and it is a measure of the departure from the spherical symmetry of the electrical charge distribution around the nucleus, ΔCq is the distribution of the quadrupolar coupling constant and indicates a structural disorder. The presence of penta-coordinated aluminium is consistent with the disordered nature of the alumina sample and is thought to originate from more highly distorted/disordered sites/components in an X-ray amorphous alumina component. Disordered or even amorphous aluminas which lack long-range order, limit the accuracy of XRD methods for quantitative phase measurements of SGAs, but are no constraint on the NMR analysis.

CONCLUDING REMARKS

Alumina fines are often regarded as a problem in aluminium smelting. However few studies examine the link between the nature of the fines and the specific process or operational problems encountered. Likewise, in the alumina refinery, considerable effort goes into understanding the generation of, but perhaps not always the nature of the fines.

Separating the fines from the bulk material and characterising these using existing techniques (such as X-ray diffraction and BET specific surface area measurements) is a useful way to observe if the fines contain over- or under calcined material. This requires little investment and has the potential return of better prediction of the behaviour of a specific SGA and required operational response, and provides a compelling argument to adopt this practice.

The use of novel analytical methods such as Environmental Scanning Electron Microscopy and very high field Solid State NMR provide new insights into the distribution of alumina phases and reveal a complex microstructure with large structural variations even within single alumina particles. These studies provide valuable and detailed insight into how the fine material can be

generated, particularly during the calcination stage in the alumina refinery, and reveal amorphous components which are in fact critically important for the properties and therefore the performance of the material in the smelter.

ACKNOWLEDGEMENTS

Financial support from Outotec Aluminium Technologies is gratefully acknowledged. A number of alumina refineries and aluminium smelters are acknowledged for providing the samples. EPSRC, Advantage West Midlands and the University of Warwick are thanked for partial funding of NMR equipment at Warwick.

REFERENCES

1. Hudson, L.K., ed. *Alumina Production*. Alcoa Research Laboratories. 1982, Aluminum Company of America: Pittsburgh, PA.
2. Taylor, A., M. *Impacts of the Refinery Process on the Quality of Smelter Grade Alumina*. in *7th International Alumina Quality Workshop*. 2005. Perth, Western Australia.
3. Saatci, A., H.-W. Schmidt, W. Stockhausen, M. Stroeder, and P. Sturm, *Attrition behavior of laboratory calcined alumina from various hydrates and its influence on SG alumina quality and calcination design.* Light Metals (Warrendale, PA, United States), 2004: p. 81-86.
4. Perander, L., C. Klett, H. Wijayaratne, M. Hyland, M. Stroeder, and J. Metson. *Impact of Calciner Technologies on Smelter Grade Alumina Microstructure and Properties*. in *8th International Alumina Quality Workshop*. 7-12 September 2008. Darwin, Australia.
5. Gillespie, A.R., M.M. Hyland, and J.B. Metson, *The surface chemistry of secondary alumina from the dry scrubbing process.* Light Metals (Warrendale, Pennsylvania), 2000: p. 345-350.
6. Welch, B.J. and G.I. Kuschel, *Crust and alumina powder dissolution in aluminum smelting electrolytes.* Jom, 2007. **59**(5): p. 50-54.
7. Candela, L. and D.D. Perlmutter, *Pore structures and kinetics of the thermal decomposition of aluminum hydroxide.* AIChE Journal, 1986. **32**(9): p. 1532-45.
8. Hyland, M., E. Patterson, and B. Welch, *Alumina structural hydroxyl as a continuous source of HF*. Light Metals (Warrendale, PA, United States), 2004: p. 361-366.
9. Metson, J.B., M.M. Hyland, and T. Groutso, *Alumina phase distribution, structural hydroxyl and performance of smelter grade aluminas in the reduction cell.* Light Metals (Warrendale, PA, United States), 2005: p. 127-131.
10. Brunauer, S., P.H. Emmett, and E. Teller, *Adsorption of gases in multimolecular layers.* Journal of the American Chemical Society, 1938. **60**: p. 309-19.
11. Barrett, E.P., L.G. Joyner, and P.P. Halenda, *The determination of pore volume and area distributions in porous substances. I. Computations from nitrogen isotherms.* Journal of the American Chemical Society, 1951. **73**: p. 373-80.
12. Ashida, T., J.B. Metson, and M.M. Hyland, *New approaches to phase analysis of smelter grade aluminas.* Light Metals (Warrendale, PA, United States), 2004: p. 93-96.

13. Roach, G.I.D., J.B. Cornell, and B.J. Griffin, *Gibbsite growth history - revelations of a new scanning electron microscope technique.* Light Metals (Warrendale, Pennsylvania), 1998: p. 153-158.
14. Baroni, T.C., B.J. Griffin, J.R. Browne, and F.J. Lincoln, *Correlation between charge contrast imaging and the distribution of some trace level impurities in gibbsite.* Microscopy and Microanalysis, 2000. **6**(1): p. 49-58.
15. Perander, L.M., Z.D. Zujovic, T. Groutso, M.M. Hyland, M.E. Smith, L.A. O'Dell, and J.B. Metson, *Characterization of metallurgical-grade aluminas and their precursors by 27Al NMR and XRD.* Canadian Journal of Chemistry, 2007. **85**(10): p. 889-897.
16. Smith, M.E., *Application of aluminum-27 NMR techniques to structure determination in solids.* Applied Magnetic Resonance, 1993. **4**(1-2): p. 1-64.
17. Slade, R.C.T., J.C. Southern, and I.M. Thompson, *Aluminum-27 nuclear magnetic resonance spectroscopy investigation of thermal transformation sequences of alumina hydrates. I. Gibbsite, Gamma-Al(OH)$_3$.* Journal of Materials Chemistry, 1991. **1**(4): p. 563-8.
18. John, C.S., N.C.M. Alma, and G.R. Hays, *Characterization of transitional alumina by solid-state magic angle spinning aluminium NMR.* Applied Catalysis, 1983. **6**(3): p. 341-346.
19. Lee, M.H., C.-F. Cheng, V. Heine, and J. Klinowski, *Distribution of tetrahedral and octahedral Al sites in gamma alumina.* Chemical Physics Letters, 1997. **265**(6): p. 673-676.
20. O'Dell, L.A., S.L.P. Savin, A.V. Chadwick, and M.E. Smith, *A ^{27}Al MAS NMR study of a sol-gel produced alumina: Identification of the NMR parameters of the θ-Al$_2$O$_3$ transition alumina phase.* Solid State Nuclear Magnetic Resonance, 2007. **31**(4): p. 169-173.
21. Slade, R.C.T., J.C. Southern, and I.M. Thompson, *Aluminum-27 nuclear magnetic resonance spectroscopy investigation of thermal transformation sequences of alumina hydrates. Part 2. Boehmite, γ-AlOOH.* Journal of Materials Chemistry, 1991. **1**(5): p. 875-9.
22. MacKenzie, K.J.D. and M.E. Smith, *Multinuclear Solid-State Nuclear Magnetic Resonance of Inorganic Materials*. 2002. 740 pp.
23. Zhou, R.S. and R.L. Snyder, *Structures and transformation mechanisms of the eta, gamma and theta transition aluminas.* Acta Crystallographica, Section B: Structural Science, 1991. **B47**(5): p. 617-30.
24. Barton, T.R., T.J. Bastow, J.S. Hall, B.J. Robson, and M.E. Smith, *Flash calcination of alumina: An NMR perspective.* Light Metals (Warrendale, Pennsylvania), 1995: p. 71-4.
25. Kunath-Fandrei, G., T.J. Bastow, J.S. Hall, C. Jaeger, and M.E. Smith, *Quantification of Aluminum Coordinations in Amorphous Aluminas by Combined Central and Satellite Transition Magic Angle Spinning NMR Spectroscopy.* Journal of Physical Chemistry, 1995. **99**(41): p. 15138-41.